Volume 15 | Number 16 | 21 August 2015 | Pages 3261–3414

Lab on a Chip

Miniaturisation for chemistry, physics, biology, materials science and bioengineering

www.rsc.org/loc

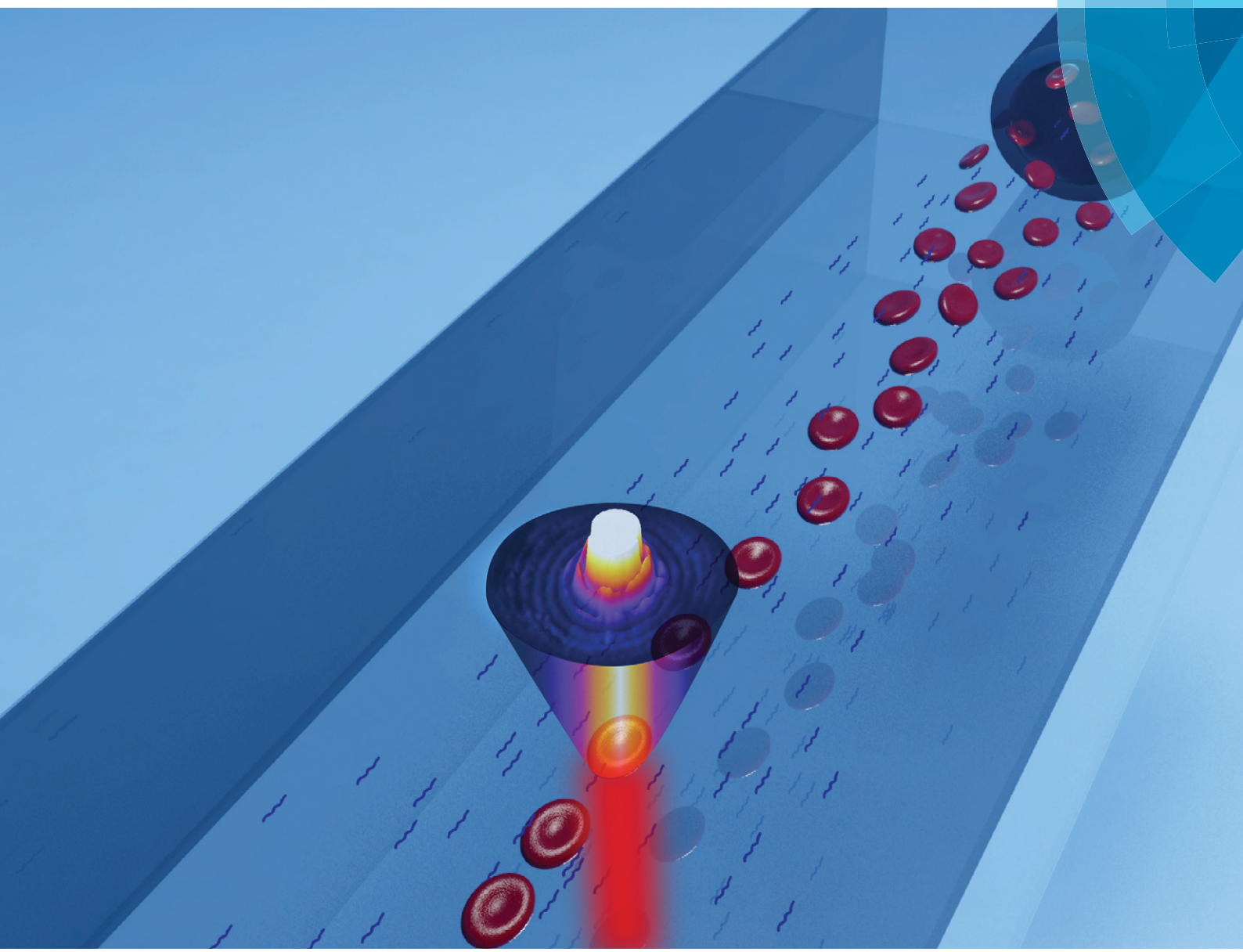

ISSN 1473-0197

ROYAL SOCIETY OF CHEMISTRY

PAPER

D. Dannhauser *et al.*

Optical signature of erythrocytes by light scattering in microfluidic flows

Lab on a Chip

PAPER

View Article Online
View Journal | View Issue

Cite this: *Lab Chip*, 2015, **15**, 3278

Optical signature of erythrocytes by light scattering in microfluidic flows†

D. Dannhauser,*[a] D. Rossi,[a] F. Causa,[b] P. Memmolo,[ac] A. Finizio,[c] T. Wriedt,[d] J. Hellmers,[e] Y. Eremin,[f] P. Ferraro[c] and P. A. Netti[ab]

Received 8th May 2015,
Accepted 2nd July 2015

DOI: 10.1039/c5lc00525f

www.rsc.org/loc

A camera-based light scattering approach coupled with a viscoelasticity-induced cell migration technique has been used to characterize the morphological properties of erythrocytes in microfluidic flows. We have obtained the light scattering profiles (LSPs) of individual living cells in microfluidic flows over a wide angular range and matched them with scattering simulations to characterize their morphological properties. The viscoelasticity-induced 3D cell alignment in microfluidic flows has been investigated by bright-field and holographic microscopy tracking, where the latter technique has been used to obtain precise cell alignment profiles in-flow. Such information allows variable cell probability control in microfluidic flows at very low viscoelastic polymer concentrations, obtaining cell measurements that are almost physiological. Our results confirm the possibility of precise, label-free analysis of individual living erythrocytes in microfluidic flows.

1 Introduction

Blood plays an essential role in human health diagnostics, as its biochemical and cellular equilibrium is extremely sensitive to the variations occurring in the body at various disease stages.[1] Thus, a fast and accurate examination of blood cell properties is essential.[2,3] The gold standard for blood cell identification is the flow cytometer. Such a complex apparatus regularly performs optical and electrical analysis or sorting of individual cells, level of protein expression or lipids at high throughput rates (up to 10 000 cells per second), typically requiring hydrodynamic sheath flow alignment and fluorescence antibody labelling.[4–6] Unlike such time-consuming and expensive fluorescence methods, advanced light scattering techniques can be used as fast, label-free measurement systems.[7]

In general, several optical inspection techniques based on tomographic or holographic approaches can be applied to characterize individual cells in-flow. The most relevant drawbacks of such techniques are their intrinsic complexity and computational costs. For instance, digital holography (DH) furnishes a light diffraction signature due to the light passing through the cells. DH is able to perform quantitative multi-focus phase-contrast imaging by using numerical refocusing criteria.[8–10] Another system is the scanning flow cytometry (SFC), where hydrodynamic sheath-flow focusing of cells is adopted. Combined with a coaxially arranged laser beam interacting with a spherical concave mirror, the scattering range of the SFC is enhanced and measured by diverse PMTs.[11,12]

If the light scattering profile (LSP) is measured by a multi-element sensor, the overall complexity of most individual cell detection systems becomes greatly simplified.[13] In fact, continuous LSP collection over a large angular range can simultaneously provide all the morphological properties of an individual naive cell, *e.g.* shape, size, refractive index (RI) and orientation in relation to the direction of the incident light. Cell characterization can be processed significantly in a simpler, more cost-effective and faster way by coupling continuous LSP measurements with individual cell interrogations in-flow.

Viscoelastic migration in microfluidic flows can be considered as a straightforward and promising method to align cells without applying any external force to the flow itself. Several alignment, sorting and classification devices for human blood cells have been fabricated over the last few years.[14–18] Nevertheless, to our knowledge, label-free characterization of living human blood cells by wide angle light

[a] *Center for Advanced Biomaterials for Healthcare@CRIB, Istituto Italiano di Tecnologia (IIT), Largo Barsanti e Matteucci 53, 80125 Naples, Italy. E-mail: david.dannhauser@iit.it*
[b] *Interdisciplinary Research Centre on Biomaterials (CRIB), Università degli Studi di Napoli "Federico II", Piazzale Tecchio 80, 80125 Naples, Italy*
[c] *CNR-ISASI Institute of Applied Sciences & Intelligent Systems "E. Caianiello", via Campi Flegrei 34, 80078 Pozzuoli, Italy*
[d] *Institut für Werkstofftechnik, Badgasteiner Str. 3, 28359 Bremen, Germany*
[e] *Particle and Process Engineering, FB4, University of Bremen, Badgasteiner Str. 3, 28359 Bremen, Germany*
[f] *Faculty of Applied Mathematics and Computer Science, Moscow State University, Lenins Hills, 119992 Moscow, Russia*

† Electronic supplementary information (ESI) available. See DOI: 10.1039/c5lc00525f

scattering, combined with precise 3D viscoelastic alignment, does not exist yet. Investigations on non-spherical blood cells – such as erythrocytes – can be used to prove our concept.

In order to gain information from a light scattering approach, it is necessary to solve the non-trivial inverse-LSP. In principle, the LSP is fitted step-by-step to a simulation curve, reducing the variance of error until a suitable result is obtained.

Several publications regarding erythrocyte simulations for scattering approaches can be found in the literature. For instance, time domain methods, such as the finite integration technique (FIT)[19] or the finite difference time domain (FDTD)[20] can be applied. Increasing interest can be noticed for the discrete dipole approximation (DDA), provided by Yurkin *et al.*[21] Eremina *et al.*[22] showed the potential of a less CPU-intensive approach, based on the discrete source method (DSM). In addition, the boundary element method (BEM) approach[23] or T-matrix method[24] can be applied to simulate the scattering effects of erythrocytes. Each of these methods has its advantages and disadvantages regarding CPU usage and simulation accuracy. In this work, we will not go into detail about the differences between the above listed simulation methods; interested readers are referred to the work of Wriedt *et al.*[19]

Here we present a direct way to investigate individual erythrocytes in microfluidic flows using a wide angle LSP approach. We applied the DDA and DSM simulation approaches to validate erythrocyte LSPs in microfluidic flows. Viscoelastic 3D cell migration – shown in our previous study for rigid latex particles[25] – was successfully applied to non-spherical living erythrocytes at diluted polymer concentrations. In order to verify cell alignment, we employed a DH method in combination with a white light standard microscope to 3D-track erythrocytes in-flow. For our DH purpose, we successfully applied a refocusing method for the 3D tracking of living cells.[26,27]

2 Materials and methods

2.1 Sample preparation

For each measurement, 3 mL of blood from a healthy donor was taken by a standard venipuncture procedure, and stored in a K_2EDTA tube (BD Vacutainer) to prevent coagulation. Samples were analysed within two hours of collection at room temperature.

Cell concentration in microfluidic flow is a critical factor for light scattering and DH analysis, due to possible multiple cell interactions. In order to obtain a suitable number of erythrocytes, the blood sample was diluted 1 million times with the microfluidic medium consisting of polyethylene oxide (PEO – M_w = 4 MDa, SIGMA-ALDRICH) dissolved in a standard phosphate-buffered saline (PBS, EUROCLONE). No glucose or other nutritious substances which can scatter light were added to the microfluidic medium, due to short experimental times. A pH and osmolarity of 7.4 and 286 mOsm L^{-1}, respectively, provided the optimal cell conditions during our DH and light scattering measurements.

2.2 Cell observation

Cell vitality was controlled before and after each light scattering measurement with a bright-field microscope (BFM, X81, OLYMPUS): a drop of pure blood was placed on a glass slide and observed with a 100× oil immersion objective.

We also performed Scanning Electron Microscopy (SEM, Ultra plus, ZEISS) analysis to examine the morphological erythrocyte parameters needed for accurate light scattering simulations. Two drops of blood were placed in poly-L-lysine coated chambers, where the platelets were activated by adding 0.2 mL of 0.2 M calcium chloride solution. Samples were subsequently fixed by adding 1 mL of 4% paraformaldehyde and 0.4% glutaraldehyde in 0.1 M sodium cacodylate buffer. After washing with 0.1 M sodium cacodylate buffer and treatment with osmium tetroxide for 16 h, the samples were dehydrated with increasing ethanol–water solutions (30%, 50%, 70%, 80%, 96%, and 100%). Finally, the samples were dried by a critical point drier (EM CPD300, LEICA), coated with a 7 nm gold film (208HR, CRESSINGTON) and observed with the SEM.

2.3 Cell alignment

Viscoelastic fluids show two different rheological characteristics under deformation, one related to the viscous fluid component, the other to the elastic solid behaviour. We measured the zero shear viscosity η_0 of scaling PEO-PBS concentrations (0.00625–0.4 g dl^{-1}), with a stress-controlled rheometer (MCR 302, ANTON PAAR, double cuvette geometry). For such diluted polymer concentrations, the longest relaxation time λ_t, considered as the main parameter for elastic fluid behaviour, cannot be measured with such a rheometer due to predominant inertia effects.

However, the general ability of cell alignment of a pressure-driven viscoelastic flowing solution strongly depends on its elastic part. The cell alignment can be expressed by a dimensionless parameter $\theta = \dot{\gamma}\lambda_t + (L/r_c)$, where $\dot{\gamma} = \Delta P r_c/(8\eta_0 L)$ is the average shear rate of the fluid, ΔP the applied pressure, L the capillary length, r_c the inner radius and β the confinement ratio between the cell radius and r_c.[28] Referring to a θ "master curve" as indicated elsewhere,[29] we calculated the λ_t of all our PEO-PBS concentrations.

Other hydrodynamic effects – the Segré–Silberberg effect or the Saffman lift force – which could shift cells to a position different from the centre line, were not considered for our polymer concentrations, due to their minor alignment influence compared to the viscoelastic force.[29,30]

2.4 Light scattering setup

We used a scattering apparatus – whose design and basic principle are shown elsewhere[25] – to accurately measure the

LSPs of differently sized individual particles or cells in microfluidic flows. The obtained LSPs span from 2–30° with an optical resolution of 0.1022°, enabling erythrocyte diameter distinction of at least 0.1 μm, due to the effort of the implemented narrow incident laser beam collimation (λ = 632.8 nm) and optimized scattered light collection system.

A variable cell throughput of up to 1.2 cells per second was obtained and analysed by a self-written Matlab routine to acquire unknown living cell properties.

2.5 LSP acquisition and simulation

Each scattered light collected by a pixel of the camera sensor was mapped to a corresponding magnitude of scattering wave vector, as shown in our previous work.[25] The average scattering intensity of each scattering angle was combined to a continuous LSP and characterized by matching the best fitting individual cell simulation. To obtain the morphological erythrocyte properties, we had to solve the inverse-LSP by calculating the possible theoretical erythrocyte scattering profiles.

Erythrocytes are biconcave disks enclosed by a thin, elastic, lipidic bilayer of around 7 nm. A mature erythrocyte is a soft, flexible and elastic cell, which has neither nucleus nor substantial internal elements. It is composed of a membrane (3% – RI = 1.3317), water (65% – RI = 1.3317) and haemoglobin (32% – RI = 1.6150).[31] In the literature, reported RIs of erythrocytes vary in a range from 1.4000 to 1.4600 for the real part, primarily related to the haemoglobin concentration, while the imaginary part can be neglected.[15,31,32] In an isotonic saline solution, human erythrocytes range from 6–9 μm in diameter, with a mean value of around 7.65 μm and a thickness of 1.42–2.84 μm.[33] Also, erythrocytes with a diameter greater than 9 μm (macrocytes) or smaller than 6 μm (microcytes) can be found in human blood.[15] It is worth knowing that the isotonicity between the medium and erythrocytes is a critical parameter for light scattering approaches. The physiological osmolarity value for erythrocytes is defined to be *circa* 290 mOsm L^{-1}, whereas in a hypotonic medium (<290 mOsm L^{-1}), cells tend to swell, while shrinkage can be observed for hypertonic conditions (>290 mOsm L^{-1}).[34]

We used a surface- and a volume-based simulation method to solve the inverse-LSP. The DDA method (ADDA v1.2) approximates the scatterer by a lattice of dipoles, using a space between the dipoles smaller than the laser wavelength. In general, the dipole number depends on numerical accuracy, geometry of the cell and RI. The dipoles have an oscillating polarization in response to both the incident plane wave and the electric fields. DDA is a robust simulation approach applicable to a wide spectrum of cell shapes.[21]

We also implemented a surface-based method using a semi-analytical DSM approach. Such a method uses an approximate solution, which is constructed by representing the electromagnetic fields as a finite linear combination of the electric and magnetic fields of multi-poles distributed inside the scatterer. DSM combines fast computational speed with the ability to calculate light scattering for any directions of incident light at the same time. In the case of erythrocytes, discrete sources are deposited in a complex plane flanked to the symmetry axis of the particle.[19] In general, relatively fast calculation times compared to DDA at similar scattering results are obtained for DSM simulations.[19,35]

Our scattering apparatus provides measurements of unpolarized scattered light. In fact, only the S_{11} element of the Mueller matrix (obtained by the ADDA software) – or the average value from the parallel and perpendicular scattering plane from the DSM simulation – was used, providing unpolarized individual cell scattering.

2.6 Holographic setup

DH in microscopy is a well-established imaging technique for the investigation of cell motility.[8–10] In particular, we exploited the ability of DH to retrieve the axial positions of the imaged cell with the aim of investigating erythrocyte alignment along the optical axis. We used a classical DH microscope with a DPSS laser (λ = 532 nm) as a light source, whose beam is coupled to an optical fibre (SF). The fibre splits the incoming laser light into an object-beam and a reference-beam. The object-beam impinges on the sample (S, *i.e.* the microfluidic chamber) before being collected by a 20× objective (MO). A CCD camera (UI-3370CP – IDS) with 512 × 2048 pixels (size 5.5 × 5.5 μm^2) is placed at an appropriate distance from the image-plane produced by the imaging objective; the CCD plane collects the digital holograms at 100 fps through a beam-splitter (BS) and the imaged field of view is 50 × 200 μm^2. A sketch of our setup is shown in Fig. 1.

Each holographic sequence is numerically processed; optical axis positions of all cells, passing the imaged field of view, are retrieved by using a suitable refocusing criterion, based on the Tamura coefficient (TC) method.[26,27] Such analysis is based on amplitude reconstructions of recorded holograms, in which cells appear in-focus when TC = $[\sigma_I/\mu_I]^{0.5}$ is minimized, with I being the amplitude image, and σ_I and μ_I

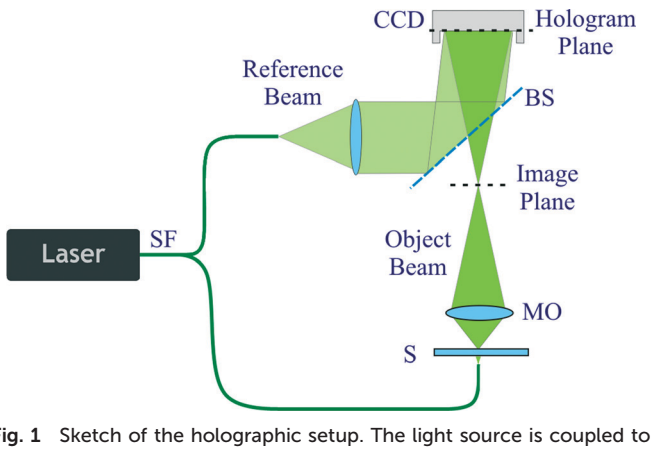

Fig. 1 Sketch of the holographic setup. The light source is coupled to an optical fibre (SF), which splits the laser light into an object- and reference-beam. The object-beam impinges on the sample (S) before both beams are collected by the CCD camera.

the image's gray-level standard deviation and mean, respectively.

3 Results and discussion

3.1 Cell observation

Precise erythrocyte measurement *via* light scattering needs preliminary assumptions of morphologic parameters. We exploited the SEM images from a proband to define the cell shape of a naive erythrocyte (see Fig. 2a). An average erythrocyte diameter of 6.91 ± 0.63 μm, with a minimum (b) and maximum (h) cell thickness of 1.15 and 1.92 μm, respectively, was measured for 57 cells and used as an input for our LSP simulation model (see Fig. 3b).

Right before each scattering measurement, detailed cell observations – in viscoelastic medium – were obtained using a BFM (see Fig. 2b). Such monitoring provides important information about cell vitality with respect to the used viscoelastic polymer. Note that a non-isotonic balance between cells and surrounding medium (hypotonic or hypertonic conditions) can be easily noticed in such a procedure. After each measurement, cell was observed again by the BFM, showing no significant deformations or evident morphological modifications (see Fig. S1c†). The pixel aspect ratio of the camera was used to analyse 25 cells of each proband, resulting in cell diameters spanning from 5.9 up to 8.6 μm (see Table 1). Furthermore, quantitative phase images were reconstructed from holographic recordings to control cell vitality and deformations in microfluidic flows (see Fig. 2c).

3.2 3D alignment measurements

Before performing light scattering measurements of individual erythrocytes, it is necessary to investigate cell alignment precisely. We measured the transverse (y-axis) and optical axis (z-axis) alignment of erythrocytes flowing in our microfluidic device for varying PEO-PBS concentrations.

A camera-based cell tracking method with the following measuring conditions was set: r_c = 25 mm, L = 40 mm, chamber profile of w = 381 mm and h = 400 mm, ΔP = 1000 mbar (see Fig. 3a).

The microfluidic device was placed on a BFM with a 20× objective, using a high sensitive CCD-camera (C11440-22CU, HAMAMATSU PHOTONICS) for data acquisition. At a free chosen position (5 mm after the capillary outlet) a minimum of 100 cells, for alternating PEO-PBS concentrations, were

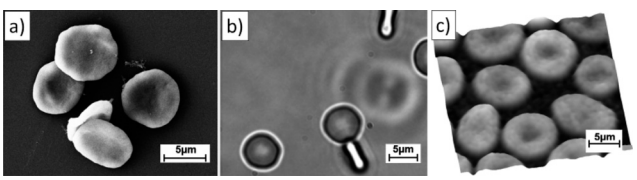

Fig. 2 SEM, BFM and DH observations of erythrocytes. a) SEM image of a cell's shape and size. b) A BFM observation in 0.2 g dl^{-1} PEO-PBS solution. c) Pseudo 3D quantitative phase image obtained by numerical reconstruction of DH images.

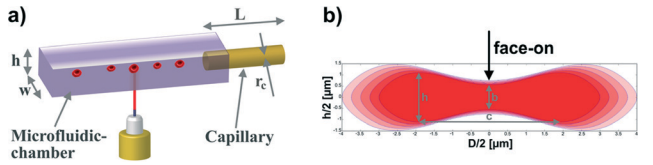

Fig. 3 a) Illustration of the microfluidic device. The round capillary enters the microfluidic chamber from the side, providing 3D particle alignment along the central axis. b) Erythrocyte cross-section of the scattering model for our DDA simulations for varying cell diameters (6–8 μm).

recorded while passing through a 94.5 μm wide area defined as m (see Fig. 4a). The frequency distributions of the tracked erythrocytes are plotted in Fig. 4b.

The highlighted green areas in Fig. 4b (12 μm wide) represent the fraction of perfectly aligned cells, important for precise scattering measurements. Our tracking routine automatically excludes all cells out of the focal plane (15 μm wide z-axis zone). As expected, reduced cell alignment with smaller PEO-PBS concentration and *vice versa* was observed. Similar data distributions can also be obtained for higher as well as lower ΔP rates (data not shown).

Precise λ_t measurement of diluted polymer solutions is challenging.[30] By measuring the percentage of perfectly aligned cells, it is possible to relate their fraction to θ and calculate the λ_t of the medium (see Fig. 4c). We cannot claim to achieve precise λ_t values, since θ is generally defined for rigid particles. We find that our λ_t trend is in good agreement with literature values,[32] even though a small absolute shift can be noticed. Comparison with η_0 measurement shows similar trends (indicated in blue) for diluted (D) polymer solutions (D – x^1) providing optimal measurement conditions for living cells. For higher polymer concentrations, where the physiological cell environment is not ensured anymore, the viscoelastic medium passes into the semi-diluted (SD) regime (SD – x^2) before reaching the entangled (E) one (E – $x^{3.4}$).

Yang *et al.*[29] show improved cell alignment of naive erythrocytes compared to stiff erythrocytes of the same size, for a highly concentrated viscoelastic medium. We confirm this behaviour with our measurements and find good agreement between λ_t values and observed cell alignment for strongly diluted polymer solutions. Our results indicate reliable cell alignment for PEO-PBS concentrations down to 0.025 g dl^{-1} in cell solution conditions similar to physiological ones, which are highly desirable for individual cell analysis.

Table 1 Erythrocyte cell diameters (in μm) reported for light scattering (LS combines DDA and DSM) and bright field microscope (BFM) measurements. The p-value shows the results obtained from t-test comparisons between the two measurement techniques

Proband	Age	Sex	Num.	LS – dia.	Num.	BFM – dia.	p-value
A	26	F	93	7.65 ± 0.44	89	7.29 ± 0.46	<0.01
B	31	F	93	7.76 ± 0.41	97	7.29 ± 0.64	<0.01
C	31	M	111	7.56 ± 0.59	88	7.34 ± 0.50	<0.01
D	30	M	110	7.57 ± 0.61	88	7.20 ± 0.51	<0.01

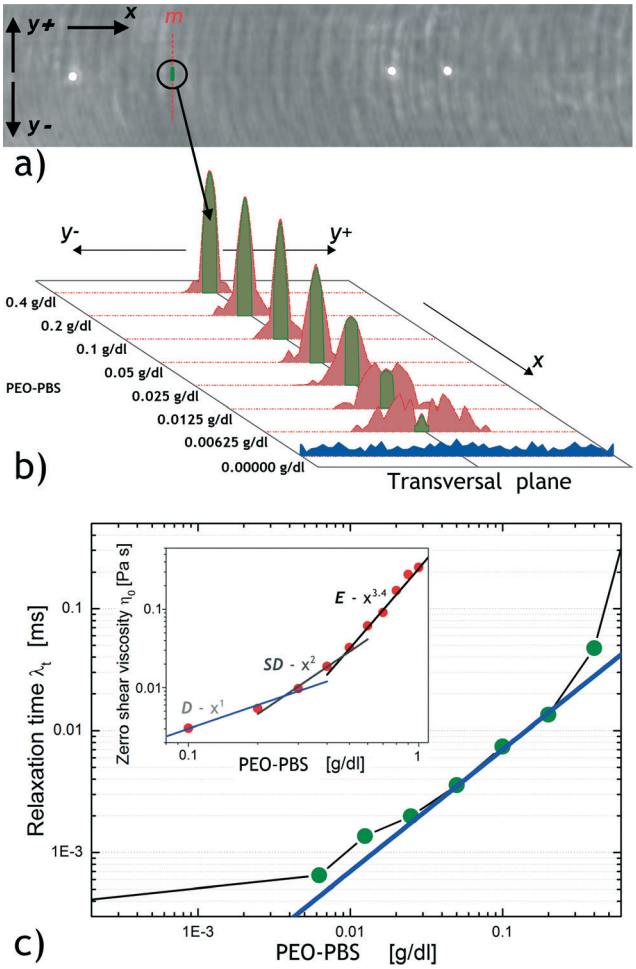

Fig. 4 Erythrocyte alignment testing for the transverse plane at varying PEO-PBS concentrations. a) Cells flowing (*x*-direction) in the microfluidic chamber (image view is 136.5 × 665.6 μm^2), with *m* the measurement plane (*y*-direction). b) Frequency distribution of cells at changing polymer concentrations. Green area indicates the fraction of cells precisely flowing in the transverse centre line. c) Calculated λ_t *vs.* polymer concentration with η_0 obtained by rheological measurements.

In addition to the transversal alignment, we studied the orientation of the flowing cells. At position *m*, more than 97% of the observed erythrocytes were transversally oriented. Thus, the results allowed us to assume a constant erythrocyte orientation at *m*, simplifying LSP simulations to an incident light angle of 0° (face-on orientation relative to the direction of the incident laser beam) (see Fig. 4a). Such an erythrocyte orientation obtains more significant LSP results compared to higher incident light angles and is generally preferred.

In order to check the alignment along the *z*-axis, holographic sequences of erythrocytes in-flow were acquired by a transmission configuration, fixing the PEO-PBS concentration at 0.2 g dl^{-1} and varying ΔP (1000 and 3000 mbar). Fig. 5 shows an example of holographic refocusing using the TC method for an individual erythrocyte with the corresponding insets showing in-focus and out-of-focus holographic reconstructions.

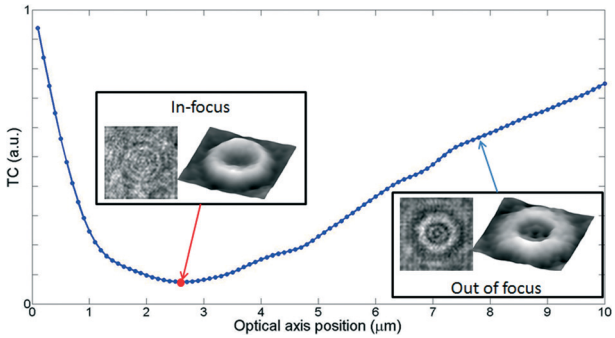

Fig. 5 TC refocusing criterion for an individually imaged cell. The minimum of TC is equal to the in-focus plane of RBC, *i.e.* its position along the *z*-axis.

The erythrocyte appeared in-focus at 2.6 μm from the centre of the microfluidic chamber, indicated by zero. Each cell of the two recorded sequences was tracked in the imaged field of view; the average position along the *z*-axis and the corresponding standard deviation were evaluated. We report these results in Fig. 6, where the normal Probability Density Functions (PDFs) are evaluated by using the calculated average and standard deviation values.

As expected, the *z*-axis position measurements show well-focused results in the case of ΔP = 3000 mbar, as demonstrated by comparing the two standard deviations ($\sigma_{1000} > \sigma_{3000}$). In addition, the comparison of their average values shows a significant *z*-axis shift from the centre line of the microfluidic chamber for the sequence recorded with ΔP = 1000 mbar (z_{1000} = −20.8 μm).

This result is related to the effect of the gravity force that becomes dominant at lower flow velocities, limiting the effectiveness of the microfluidic focusing along the *z*-axis. In order to overcome this issue, a suitable ΔP level for the given polymer concentrations is needed to guarantee an accurate 3D alignment of flowing erythrocytes over long measurement distances. In fact, our investigation leads to establish a ΔP value equal to at least 3000 mbar at a given PEO-PBS concentration of 0.2 g dl^{-1} to provide the minimum cell variance inflow. Such high cell velocity results in perfect alignment with

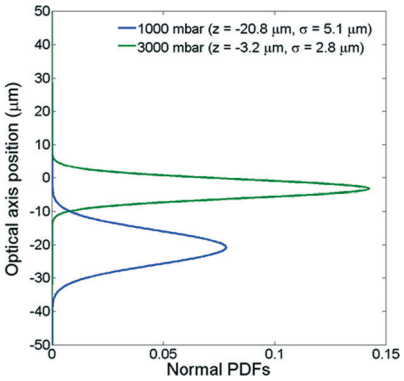

Fig. 6 Normal PDFs for two sequences of flowing erythrocytes, measured with different pressures (ΔP = 1000 and 3000 mbar).

small variance over long microfluidic flow distances, for both the *y*- and the *z*-axis trajectories.

However, a reasonable compromise between cell velocity and alignment variance should be set, to avoid possible cell deformations in-flow and to respect the performance limitation of the used measurement system.

3.4 Light scattering measurements

All light scattering measurements were performed at room temperature, with the previously described microfluidic device (see Fig. 3a). We used a PEO-PBS concentration of 0.2 g dl^{-1} and a ΔP of 1000 mbar, resulting in suitably aligned cells at a velocity of 100 μm s^{-1}. Such an erythrocyte velocity allows an achievable data acquisition configuration and avoids possible cell deformations in-flow, occurring at high $\dot{\gamma}$ rates. In view of the previously mentioned alignment results, our scattering apparatus was calibrated to the *z*-axis position of the used ΔP value before each measurement, ensuring optimal microfluidic flow conditions. Note that acquisitions at higher ΔP values, resulting in even smaller cell variances in microfluidic flow, are limited by the camera performance.

To obtain the unknown morphological erythrocyte properties, we had to solve the inverse-LSP. We calculated the theoretical LSP from 5 up to 10 μm diameter, with a relative RI (rRI) of 1.0513 for the DDA and DSM-method; we used the shape model of Fung *et al.*[33] and an extension of the shape model of Kuchel *et al.*,[35] respectively. We do not claim that the used shape models are the best fitting ones for all measured erythrocytes; these were just convenient and broad parameterization methods, which produce realistically-looking shapes (see Fig. 3b).[36]

The LSP simulation changed due to different erythrocyte shapes, as calculated by the DSM and DDA approach, which are shown in Fig. 7. The SEM parameters for DDA simulations were used with 0.250 (h/D), 0.170 (b/D) and 0.500 (c/D), according to the definition of Fig. 3b, while for the model of Fung *et al.* (0.370, 0.187, and 0.638),[33,37] as well as Kuchel *et al.* (0.275, 0.125, and 0.625),[35] literature parameters were used.

We observed that by alternating the rRI in the range from 1.0333 to 1.0963 and the cell thickness from 1.35 to 3.37 μm at a given cell diameter of 7.5 μm, an absolute LSP intensity shift occurred, without effectively influencing the LSP oscillation form, as seen in Fig. 7d. DSM and DDA simulations calculated with the model of Fung *et al.* showed equivalent LSP curves until the size of 10 μm for our scattering range (data not shown). Such a perfect matching between both simulation techniques – with equal erythrocyte shape models – for LSP curves from 5 to 10 μm has not been published yet in the literature and proves the validity of both simulation approaches.

The erythrocytes for each proband were characterized, where one exemplary LSP for each proband overlaid by its corresponding simulation curve for DSM (Fung-shape) and DDA (SEM-shape) simulation is shown in Fig. 8.

The minor LSP difference between the simulation approaches is due to the different erythrocyte shapes. Each LSP was matched with all pre-calculated simulation curves for both simulation approaches to obtain the best fitting one. No significant differences between the two simulation approaches were recognized. The LSP analysing procedure was focused to best match the angular section from 5–20°, due to the more significant scattering oscillations in this range. The minima and the maxima positions of each oscillation curve were taken into account to classify the best matching pre-calculated LSP curve. In case of mismatching among all simulations, the LSP was excluded from data analysis. In addition, an asymmetric erythrocyte shape measurement can provoke a noisy LSP and – in the worst cases – also blur individual oscillation structures, leading to its exclusion.

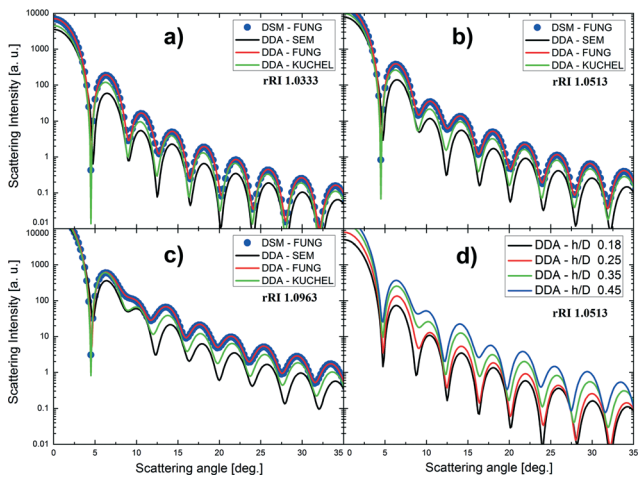

Fig. 7 LSP simulations (DSM and DDA approach) for our scattering apparatus at varying input parameters. Plots a), b) and c) show the rRI influence on the LSP simulation for different erythrocyte models (SEM, FUNG, KUCHEL), while in d) the influence of the cell thickness is highlighted. All curves are plotted for a cell diameter of 7.5 μm.

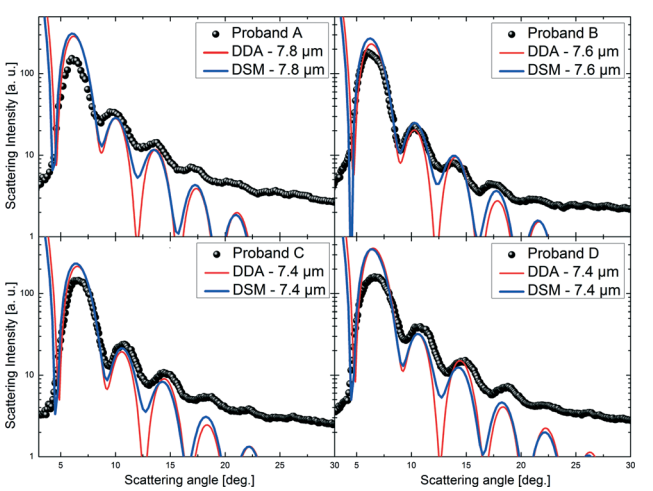

Fig. 8 LSP of an individual erythrocyte for each proband, obtained by our scattering apparatus. The red line illustrates the scattering simulation based on DDA simulations.

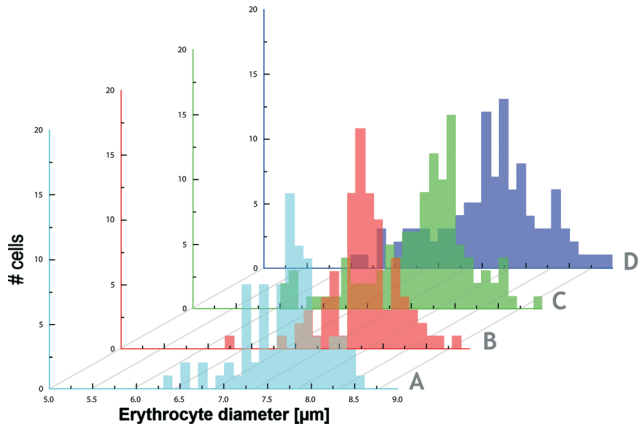

Fig. 9 Erythrocyte diameter distribution measured in microfluidic flow by our light scattering apparatus. Histograms a) and b) show female probands, while in c) and d) male probands are presented.

Indeed, in view of the minor influence of rRI and cell thickness on the LSP oscillation form – for our measurement conditions – the erythrocyte diameter remained the only significant parameter for precise LSP characterizations. The average diameter of an erythrocyte population, together with its variance, can be easily referred to the clinically measured "red blood cell distribution width" (RDW) value,[1] giving useful information about the health status of a patient. We summarized the average erythrocyte LSP and BFM diameters in Table 1.

In fact, good agreement between the measured and simulated LSPs was obtained, allowing precise living erythrocyte measurements in microfluidic flows. A healthy erythrocyte diameter typically lies between 6 and 9 µm. Diameters obtained by our light scattering apparatus (~7.64 µm) were generally slightly larger compared to BFM observations (~7.28 µm). Such a small discrepancy can be associated with the applied LSP acquisition technique, which in our case is based on the scattering symmetry. The results were analysed using the *t*-test, showing *p*-values below 0.01, making data comparison possible.

All cell diameters of each proband, obtained by our light scattering apparatus and analysed by matching the best fitting simulation method, are graphically summarized in Fig. 9. We found that the majority of the measured erythrocytes are between 7 and 8.3 µm in diameter, which is in good agreement with the values found in the literature.[19,31,33] Probands A and B show a narrower diameter distribution compared to the other probands, while slightly higher average diameters are noticed.

4 Conclusions

We have presented an accurate, straightforward, label-free light scattering analysis of individual erythrocytes in microfluidic flows. Our analyses are possible due to the precise 3D alignment of individual cells taking advantage of the viscoelasticity effects in strongly diluted PEO-PBS solution. It is important to note that – for the first time – low concentrations of PEO are adopted for 3D microfluidic alignment. PEO is an inexpensive, biocompatible and non-toxic commercial polymer.

Our measured LSPs match with the predicted DSM and DDA simulation profiles, solving the inverse-LSP and obtaining the unknown erythrocyte dimensions. For the first time, perfect LSP agreement from 5 to 10 µm erythrocyte diameter between the two simulation approaches has been found. The diameter values from four different donors are between 7 and 8.3 µm, with an overall average value of ~7.64 µm, which is in good agreement with the literature values. Our results demonstrate the ability of a rapid and cost-effective way to measure the average dimensions of an erythrocyte population, together with its variance (clinically referred as RDW). Such a variation parameter can be easily related to the health status of a patient.

Our results show a valuable approach for the direct light scattering measurement of non-spherical cells. We foresee, on the basis of the results reported in this work, the possibility in the near future to compare between physiological and pathological cell status, opening the scenario of completely label-free diagnostics for blood diseases.

References

1 M. M. Wintrobe and J. P. Greer, *Wintrobe's clinical hematology*, Wolters Kluwer Health/Lippincott Williams & Wilkins, Philadelphia, 2009.
2 L. Miccio, P. Memmolo, F. Merola, P. A. Netti and P. Ferraro, *Nat. Commun.*, 2015, **6**(6502), 1–7.
3 F. Merola, P. Memmolo, L. Miccio, V. Bianco, M. Paturzo and P. Ferraro, *Proc. IEEE*, 2015, **103**(2), 192–204.
4 C. B. Black, T. D. Duensing, L. S. Trinkle and R. T. Dunlay, *Assay Drug Dev. Technol.*, 2011, **9**(1), 13–20.
5 D. Barnett, B. Walker, A. Landay and T. N. Denny, *Nat. Rev. Microbiol.*, 2008, **6**, S7–S15.
6 A. E. Vasdekis and G. Stephanopoulos, *Metab. Eng.*, 2015, **27**, 115–135.
7 X. Su, S. E. Kirkwood, M. Gupta, L. Marquez-Curtis, Y. Qiu, A. Janowska-Wieczorek, W. Rozmus and Y. Y. Tsuin, *Opt. Express*, 2011, **19**(1), 387–398.
8 P. Memmolo, V. Bianco, F. Merola, L. Miccio, M. Paturzo and P. Ferraro, *IEEE Photonics J.*, 2014, **6**(2), 701106.
9 L. Miccio, P. Memmolo, F. Merola, S. Fusco, V. Embrione, A. Paciello, M. Ventre, P. A. Netti and P. Ferraro, *Lab Chip*, 2014, **14**, 1129–1134.
10 F. Merola, L. Miccio, P. Memmolo, G. Di Caprio, A. Galli, R. Puglisi, D. Balduzzi, G. Coppola, P. A. Netti and P. Ferraro, *Lab Chip*, 2013, **13**, 4512–4516.
11 V. P. Maltsev and K. A. Sem'yanov, *Characterisation of bioparticles from light scattering*, Walter de Gruyter, 2004.
12 M. A. Yurkin, K. A. Semyanov, P. A. Tarasov, A. V. Chernyshev, A. G. Hoekstra and V. P. Maltsev, *Appl. Opt.*, 2005, **44**(25), 5249–5256.
13 F. Ferri, *Rev. Sci. Instrum.*, 1997, **68**(6), 2265–2274.

14 T. F. Wu, Z. Mei and Y. H. Lo, *Lab Chip*, 2012, **12**(19), 3791–3797.
15 K. W. Seo, Y. R. Ha and S. J. Lee, *Appl. Phys. Lett.*, 2014, **104**(21), 213702.
16 E. J. Lim, T. J. Ober, J. F. Edd, G. H. McKinley and M. Toner, *Lab Chip*, 2012, **12**(12), 2199–2210.
17 S. C. Hur, H. T. K. Tse and D. Di Carlo, *Lab Chip*, 2010, **10**(3), 274–280.
18 B. S. Lee, Y. U. Lee, H. S. Kim, T. H. Kim, J. Park, J. G. Lee, J. Kim, H. Kim, W. G. Lee and Y. K. Cho, *Lab Chip*, 2011, **11**(1), 70–78.
19 T. Wriedt, J. Hellmers, E. Eremina and R. Schuh, *J. Quant. Spectrosc. Radiat. Transfer*, 2006, **100**(1), 444–456.
20 J. Q. Lu, P. Yang and X. H. Hu, *J. Biomed. Opt.*, 2005, **10**(2), 024022–02402210.
21 M. A. Yurkin and A. G. Hoekstra, *J. Quant. Spectrosc. Radiat. Transfer*, 2011, **112**(13), 2234–2247.
22 E. Eremina, Y. Eremin and T. Wriedt, *Opt. Commun.*, 2005, **244**(1), 15–23.
23 S. V. Tsinopoulos and D. Polyzos, *Appl. Opt.*, 1999, **38**(25), 5499–5510.
24 A. M. Nilsson, P. Alsholm, A. Karlsson and S. Andersson-Engels, *Appl. Opt.*, 1998, **37**(13), 2735–2748.
25 D. Dannhauser, G. Romeo, F. Causa, I. De Santo and P. A. Netti, *Analyst*, 2014, **139**(20), 5239–5246.
26 P. Memmolo, C. Distante, M. Paturzo, A. Finizio, P. Ferraro and B. Javidi, *Opt. Lett.*, 2011, **36**, 1945–1947.
27 P. Memmolo, M. Iannone, M. Ventre, P. A. Netti, A. Finizio, M. Paturzo and P. Ferraro, *Opt. Express*, 2012, **20**, 28485–28493.
28 G. Romeo, G. D'Avino, F. Greco, P. A. Netti and P. L. Maffettone, *Lab Chip*, 2013, **13**(14), 2802–2807.
29 S. Yang, S. S. Lee, S. W. Ahn, K. Kang, W. Shim, G. Lee, G. K. Hyun and J. M. Kim, *Soft Matter*, 2012, **8**(18), 5011–5019.
30 F. Del Giudice, G. D'Avino, F. Greco, I. De Santo, P. A. Netti and P. L. Maffettone, *Lab Chip*, 2015, **15**, 783–792.
31 M. Hammer, D. Schweitzer, B. Michel, E. Thamm and A. Kolb, *Appl. Opt.*, 1998, **37**(31), 7410–7418.
32 A. N. Shvalov, J. T. Soini, A. V. Chernyshev, P. A. Tarasov, E. Soini and V. P. Maltsev, *Appl. Opt.*, 1999, **38**(1), 230–235.
33 Y. C. Fung, W. C. Tsang and P. Patitucci, *Biorheology*, 1981, **18**(3–6), 369.
34 P. Memmolo, L. Miccio, F. Merola, O. Gennari, P. A. Netti and P. Ferraro, *Cytometry, Part A*, 2014, **85**(12), 1030–1036.
35 P. W. Kuchel and E. D. Fackerell, *Bull. Math. Biol.*, 1999, **61**(2), 209–220.
36 E. Eremina, J. Hellmers, Y. Eremin and T. Wriedt, *J. Quant. Spectrosc. Radiat. Transfer*, 2006, **102**(1), 3–10.
37 K. V. Gilev, E. Eremina, M. A. Yurkin and V. P. Maltsev, *Opt. Express*, 2010, **18**(6), 5681–5690.